J|A|C|S
ARTICLES
Published on Web 04/26/2002

Thermal Dissociation of Protein−Oligosaccharide Complexes in the Gas Phase: Mapping the Intrinsic Intermolecular Interactions

Elena N. Kitova, David R. Bundle, and John S. Klassen*

Contribution from the Department of Chemistry, University of Alberta, Edmonton, Alberta, Canada T6G 2G2

Received October 2, 2001

Abstract: Blackbody infrared radiative dissociation (BIRD) and functional group replacement are used to map the location and strength of hydrogen bonds between an antibody single chain fragment (scFv) and its natural trisaccharide receptor, α-D-Gal*p* (1→2)[α-D-Abe*p* (1→3)]α-D-Man*p*1→OMe (**1**), in the gaseous, multiply protonated complex. Arrhenius activation parameters (E_a and A) are reported for the loss of **1** and a series of monodeoxy trisaccharide congeners (**5**−**8** ≡ **tri**) from the (scFv + **tri** + 10H)$^{+10}$ complex. The energetic contribution of the specific oligosaccharide OH groups to the stability of the (scFv + **1** + 10H)$^{+10}$ complex is determined from the differences in E_a measured for the trisaccharide analogues and **1** (55.2 kcal/mol). A decrease of 6 to11 kcal/mol in E_a, measured for the monodeoxy trisaccharides, indicates that the deleted OH groups interact strongly with the scFv and that they account for a majority of the stabilizing intermolecular interactions. A partial map of the hydrogen bond donor/acceptor groups of **1** and the strength of the interactions is presented for the protonated +10 complex. A comparison of the gas-phase map with the crystal structure indicates that significant structural differences exist. The hydroxyl groups located outside of the binding pocket, and exposed to solvent in solution, participate in new protein−oligosaccharide hydrogen bonds in the gas phase. The decrease in kinetic and energetic stability of the (scFv + **2** + *n*H)$^{n+}$ complex with increasing charge-state is attributed to conformational differences in the binding region induced by electrostatic repulsion. The similarity in the Arrhenius parameters for the +9 and +10 charge states suggests that repulsion effects on the structure of the binding region are negligible below +11.

Introduction

The association of molecules via the concerted action of noncovalent interactions forms the basis for molecular recognition in biological systems. Identifying and understanding the forces responsible for binding affinity and, consequently specificity, are of paramount importance. The relationship between structure and function is, however, poorly understood. One of the major obstacles to rationalizing binding affinities in an aqueous environment lies in an incomplete understanding of the structural and energetic role played by the solvent. It is recognized that the reorganization of water molecules located at the binding sites prior to association, represents a significant, and in some cases dominant, component of the association free energy (ΔG_{assoc}).[1] The free energy is the sum of contributions from intrinsic interactions (ΔG_{intrin}) between the two solute molecules and those originating from solvent reorganization (ΔG_{solv}), both of which must be known to predict binding affinities:

$$\Delta G_{assoc} = \Delta G_{intrin} + \Delta G_{solv} = (\Delta H_{intrin} - T\Delta S_{intrin}) + (\Delta H_{solv} - T\Delta S_{solv}) \quad (1)$$

These thermodynamic parameters for association in the aqueous phase are readily determined using techniques such as isothermal titration calorimetry, and comparative data provide insight into the contribution of specific functional groups or structural features to the association process. However, interpretation of the thermochemical parameters at the molecular level is uncertain since they reflect the intrinsic and solvent reorganization components. As a result, rational strategies for drug design have been largely replaced by combinatorial approaches, while higher-order protein structure is more conveniently described by empirical rather than theoretical models.

Computational and gas-phase studies of biomolecular complexes are promising routes to partition the intrinsic and solvent effects. Gas-phase research of biological molecules and their complexes is a field in its infancy, and the extent to which gas-phase studies are relevant to solution properties is unclear. Direct structural techniques, such as NMR or X-ray crystallography, are unavailable. Instead, indirect methods such as ion mobility

* To whom correspondence should be addressed. E-mail: john.klassen@ualberta.ca.

(1) (a) Rand, R. P. *Science* **1992**, *256*, 618−618. (b) Lemieux, R. U. *Acc. Chem. Res.* **1996**, *29*, 373−380. (c) Oas, T. G.; Toone, E. J. In *Advances in Biophysical Chemistry*; Bush, C. A., Ed.; JAI Press Inc.: Greenwich, CT, 1997; Vol. 6, pp 1−52.

10.1021/ja017213o CCC: $22.00

measurements,[2−6] ion−molecule[7−9] and ion dissociation reactions[10−14] are being used to evaluate structure. There is evidence that, in some cases, proteins and protein−ligand complexes transferred from solution to the gas phase using the gentle ES process retain aspects of higher-order solution structure. For protein−ligand complexes, a correlation between the gas-phase stability (kinetic) of structurally related protein−ligand complexes and their binding enthalpies or dissociation activation energies measured in solution has served as evidence for the retention of the specific intermolecular interactions upon transfer from solution to the gas phase. Such a correlation has been reported for several protein complexes including heme-binding proteins[12] and OppA−peptide complexes.[13] The degree of correlation will reflect, in part, the nature of the interactions responsible for association in solution. In the aforementioned cases, electrostatic interaction dominates and the degree of correlation is high. In contrast, complexes believed to involve considerable hydrophobic interaction are not expected to exhibit a correlation since different intermolecular interactions will dominate in the gas phase. For example, a study of the kinetic stability of gaseous complexes of carbonic anhydrase II with para-substituted benzenesulfonomides found no correlation with the solution phase association constants. Instead, the gas-phase stability appeared to be sensitive to the size of the polar group at the *para* position.[14] This result was attributed to intermolecular interactions between the polar tail and the protein in the gas phase. These interactions are absent in solution since these groups are efficiently solvated. The results from these studies suggest that the gas-phase stability of protein complexes can, in some cases, provide information about the nature of the intrinsic interactions in solution. However, studies carried out with well defined and, ideally, thermal internal energy distributions are needed to delineate the energetic and entropic contribution to the dissociation kinetics and to strengthen conclusions regarding structure and binding energies. Thermal dissociation studies will also provide much needed insight into the decomposition mechanisms of protein−ligand complexes and advance our understanding of the nature and the strength of the intermolecular interactions present in the absence of solvent.

Time-resolved thermal dissociation studies of large, isolated gaseous ions can be performed using the blackbody infrared radiative dissociation (BIRD) technique.[15,16] With BIRD, ions are trapped in the ion cell of the FT-ICR and are heated to the point of dissociation by the absorption of blackbody photons emitted from the surroundings (i.e., ion cell and vacuum chamber). For large ions with many IR-active modes, the rate of radiative absorption and emission may be rapid compared to the rate of dissociation; the ions may then thermally equilibrate with the radiant flux and adopt a Boltzmann distribution of internal energies. Under these conditions, the thermal dissociation rate constants can be measured.[16b,c] From the temperature dependence of the rate constants, the Arrhenius activation energy (E_a) and preexponential factor (A) can be determined. BIRD has been used to determine Arrhenius activation parameters for a number of biopolymers, including protonated peptides[16d,16e] and small proteins,[16b] and deprotonated oligonucleotides.[16f] BIRD has also been used to study the kinetics and energetics for the dissociation of a number of noncovalent biomolecular complexes. Arrhenius parameters have been determined for the loss of heme from heme−globin complexes,[17] the dissociation of DNA duplexes into single strands,[18] and for the loss of protein subunits from protein assemblies.[19,20]

Here, we report the first thermal dissociation kinetic and energetic measurements, carried out using the BIRD technique, for a series of structurally related protein−ligand complexes in the gas phase. Oligosaccharide complexes of the single-chain antibody fragment (scFv), based on the carbohydrate-binding antibody Se155-4 were chosen for this study. The Se155-4 monoclonal antibody exhibits specificity for the trisaccharide (α-D-Gal*p* (1→2)[α-D-Abe*p* (1→3)]α-D-Man*p*1→OMe (**1**) epitope of *Salmonella* (group B O-antigen). The association thermodynamics for Se155-4 with a variety of oligosaccharides have been extensively investigated in solution,[21] and these data provide a useful comparison with the gas-phase stabilities measured in the present work.

As is typical of protein−oligosaccharide complexes, hydrogen bonding between the oligosaccharide hydroxyl groups and the amino acids, as well as water-mediated hydrogen bonds, represent the dominant solute−solute interactions in the antibody−carbohydrate complex in solution. These intermolecular hydrogen bonds are expected to strengthen upon removal of water and some or all of the specific interactions retained in the gas phase. Shown in Figure 1 is the hydrogen bond scheme for the scFv−**1** complex inferred from the crystal structure[22] and binding studies.[21] The buried Abe residue provides the dominant source of binding enthalpy in the complex. The Gal and Man residues contribute only modestly to association. Prior to binding, several hydrogen-bonding sites are occupied by water molecules.[23] For association to occur, some of these waters must

(2) Valentine, S. J.; Clemmer, D. E. *J. Phys. Chem. B* **1997**, *101*, 3891−3900.
(3) Valentine, S. J.; Clemmer, D. E. *J. Am. Chem. Soc.* **1997**, *119*, 3558−3566.
(4) Shelimov, K. B.; Clemmer, D. E.; Hudgins, R. R.; Jarrold, M. F. *J. Am. Chem. Soc.* **1997**, *119*, 2240−2248.
(5) Shelimov, K. B.; Jarrold, M. F. *J. Am. Chem. Soc.* **1997**, *119*, 2987−2994.
(6) Mao, Y.; Woenckhaus, J.; Kolafa, J.; Ratner, M. A.; Jarrold, M. F. *J. Am. Chem. Soc.* **1999**, *121*, 2712−2721.
(7) Wood, T. D.; Chorush, R. A.; Wampler, F. M.; Little, D. P.; O'Connor, P. B.; McLafferty, F. W. *Proc. Natl. Acad. Sci. U.S.A.* **1995**, *92*, 2451−2454.
(8) McLafferty, F. W.; Guan, Z.; Haupts, U.; Wood, T. D.; Kelleher, N. L. *J. Am. Chem.* Soc. **1998**, *120*, 4732−4740.
(9) Covey, T. R.; Douglas, D. J. *J. Am. Soc. Mass Spectrom.* **1993**, *4*, 616−623.
(10) Loo, J. A. *Mass Spectrom. Rev.* **1997**, *16*, 1−23.
(11) Veenstra, T. D. *Biochem. Biophys. Res. Commun.* **1999**, *257*, 1−5.
(12) Hunter, C. L.; Mauk, A. G.; Douglas, D. J. *Biochemistry* **1997**, *36*, 1018−1025.
(13) Rostom, A. A.; Tame, J. R. H.; Ladbury, J. E.; Robinson, C. V. *J. Mol. Biol.* **2000**, *296*, 269−279.
(14) Wu, Q.; Gao, J.; Joseph-McCarthy, D.; Sigal, G. B.; Bruce, J. E.; Whitesides, G. M.; Smith, R. D. *J. Am. Chem. Soc.* **1997**, *119*, 1157−1158.
(15) Tholmann, D.; Tonner, D. S.; McMahon, T. B. *J. Phys. Chem.* **1994**, *98*, 2002−2004.
(16) (a) Price, W. D.; Schnier, P. D.; Williams, E. R. *Anal. Chem.* **1996**, *68*, 859−866. (b) Price, W. D.; Schnier, P. D.; Jockusch, R. A.; Strittmatter, E. F.; Williams, E. R. *J. Am. Chem. Soc.* **1996**, *118*, 10640−10644. (c) Price, W. D.; Williams, E. R. *J. Phys. Chem. A* **1997**, *101*, 8844−8852. (d) Price, W. D.; Schnier, P. D.; Williams, E. R. *Anal. Chem.* **1996**, *68*, 859−866. (e) Schnier, P. D.; Price, W. D.; Jockusch, R. A.; Williams, E. R. *J. Am. Chem. Soc.* **1996**, *118*, 7178−7189. (f) Klassen, J. S.; Schnier, P. D.; Williams, E. R. *J. Am. Soc. Mass Spectrom.* **1998**, *9*, 1117−1124.
(17) Cross, S. G.; Zhao, Y.; Williams, E. R. *J. Am. Soc. Mass Spectrom.* **1997**, *8*, 519−524.
(18) Schnier, P. D.; Klassen, J. S.; Strittmatter, E. E.; Williams, E. R. *J. Am. Chem. Soc.* **1998**, *120*, 9605−9613.
(19) Felitsyn, N.; Kitova, E. N.; Klassen, J. S. *Anal. Chem.* **2001**, *73*, 4647−4661.
(20) Felitsyn, N.; Klassen, J. S. Manuscript in preparation.
(21) Bundle, D. R.; Eichler, E.; Gidney, M. A. J.; Meldal, M.; Ragauskas, A.; Sigurskjold, B. W.; Sinnot, B.; Watson, D. C.; Yaguchi, M.; Young, N. M. *Biochemistry* **1994**, *33*, 5172−5182.
(22) Zdanov, A.; Li, Y.; Bundle, D. R.; Deng, S.-J.; MacKenzie, C. R.; Narang, S. A.; Young, M. N.; Cygler, M. *Proc. Natl. Acad. Sci. U.S.A.* **1994**, *91*, 6423−6427.

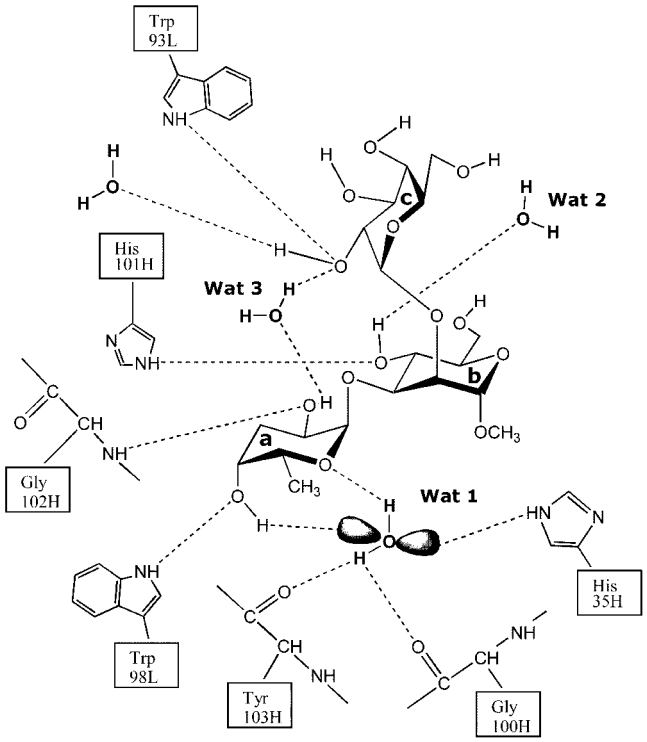

Figure 1. Hydrogen-bond map obtained from the crystal structure of complex of the Se155-4 antibody single chain fragment and α-D-Gal*p* (1→2)[α-D-Abe*p* (1→3)]α-D-Man*p*1→OMe (**1**).[22] Amino acid residues numbered according to the Kabat scheme.

be displaced from the sugar surface and the epitope binding region of the protein and returned to the bulk solution. Consequently, solvent displacement is believed to contribute significantly to ΔG°_{assoc}.[24] Structured water also plays an important role in these complexes. A single water molecule (Wat 1) located at the base of the binding pocket, as revealed by the crystal structure of (scFv + **1**), mediates hydrogen bonding between the scFv and the Abe C-4 OH group. Three additional water molecules, on the periphery of the interface, are also observed. Crystal structures obtained for the Se155-4 Fab-**1** complex indicate some variability in the ligand conformation. In one of the conformers, Wat 3 was not observed, and a direct sugar−sugar hydrogen bond replaced the water-mediated hydrogen bond.[25]

The goal of the present work was to elucidate the nature and strength of the binding interactions in the (scFv + **1**) complex in the absence of solvent. To our knowledge, this is the first attempt to map AND quantify the intermolecular interactions that stabilize a protein−ligand complex in the absence of solvent. Comparison of the gas-phase map with solution-binding studies and the solved crystal structure provides new insights into the structural differences that exist between the complex in the gas phase and that in the condensed phase. The influence of charge state on the stability of the complexes was also investigated. The (scFv + Tal[Abe]Man)$^{n+}$ complex was used to examine the influence of charge on binding. Five charge states (n = 9−13) of the multiply protonated complex and two charge states (n = 10, 11) of the monosodiated complex were investigated.

Experimental Section

Mass spectra were obtained using an ApexII 47e Fourier transform ion cyclotron resonance (FT-ICR) mass spectrometer (Bruker, Billerica MA) with a modified external nanoelectrospray source (Analytica, Branford). This instrument has been previously described,[19] and only a brief overview is given here. Nanoelectrospray was performed using an aluminosilicate capillary (0.68 mm i.d.), pulled to approximately 20 μm o.d. and 1−5 μm i.d. at one end using a micropipet puller (Sutter Instrument Co.). The electric field required to spray the solution was established by applying a voltage of 800−1000 V to a platinum wire inserted inside the glass tip. The solution flow rate ranged from 5 to 100 nL/min, depending on diameter of the nanoelectrospray tip, the electrospray voltage, and the composition of the solution. The droplets and gaseous ions produced by nanoES were introduced into the vacuum chamber of mass spectrometer through a stainless steel capillary (i.d. 0.42 mm) maintained at a temperature of 150 °C. The ion/gas jet sampled by the capillary (52 V) was transmitted through a skimmer (4 V) and stored, electrostatically, in a hexapole. Ions were accumulated in the hexapole for 2−5 s, depending on the ion intensities, then ejected and accelerated (∼−2700 V) through the fringing field of a 4.7 T superconducting magnet, decelerated and introduced into the ion cell. The trapping plates of the cell were maintained at a constant potential of 1.3 V throughout the experiments. The typical base pressure for the instrument was $\sim 5 \times 10^{-10}$ mbar.

Data acquisition was controlled by an SGI R5000 computer running the Bruker Daltonics XMASS software, version 5.0. Mass spectra were obtained using standard experimental sequences with chirp broadband excitation. Isolation of the parent ions for the BIRD experiments was achieved using single rf frequency and broadband rf sweep excitation. The isolated ions were stored inside the heated cell for variable reaction times prior to excitation and detection. The excitation pulse length was varied between 10 and 15 μs and the power of excitation pulse was varied as to maximize the intensity of the ion signal. The time-domain spectra, consisting of the sum of 10−30 transients containing 128 K data points per transient, were subjected to one zero-fill prior to Fourier transformation.

The temperature of the ion cell was controlled with two external flexible heating blankets placed around the vacuum tube in the vicinity of the cell. In a separate experiment, the temperature inside the cell, measured by a thermocouple placed temporarily inside the cell, was calibrated against the temperature measured by eight thermocouples placed on the outside of the vacuum tube. Using this approach, calibration plots were generated for cell temperatures ranging from 25 to 175 °C.

Recombinant scFv, expressed in *Escherichia coli*, was isolated and purified as described previously.[22] The purified scFv was dissolved in 1 mM aqueous ammonium acetate buffer (pH = 6.7) at a concentration of $\sim 10^{-5}$ M. The oligosaccharide ligand concentration ranged from 10^{-3} to 10^{-5} M, depending on the magnitude of the binding constant in solution.

The semiempirical calculations were performed using HyperChem (v. 6.02, Hypercube Inc., Gainesville, FL), and the Hartree−Fock (HF) calculations were performed using GAMESS US.[26] Energy minimization was first performed using the AM1 method, followed by further minimization at the HF level using the 6-31G** basis set. The initial histidine structure used for the HF calculation was obtained using the

(23) Cygler, M.; Bundle, D. R. Unpublished results.
(24) (a) Lemieux, R. U.; Delbaere, L. T. J.; Beierbeck, H.; Spohr, U. In *Host−Guest Molecular Interactions: From Chemistry to Biology*; Ciba Foundation Symposium; Wiley: Chichester, 1991; Vol. 158, pp 231−248. (b) Isbister, B. D.; St. Hilaire, P. M.; Toone, E. J. *J. Am. Chem. Soc.* **1995**, *117*, 12877−12878. (c) Chervenak, M. C.; Toone, E. J. *J. Am. Chem. Soc.* **1994**, *116*, 10533−10539.
(25) Cygler, M.; Rose, D. R.; Bundle, D. R. *Science* **1991**, *253*, 442−446.
(26) (a) Schmidt, M. W.; Baldridge, K. K.; Boatz, J. A.; Jensen, J. H.; Koseki, S.; Gordon, M. S.; Ngueyen, K. A.; Windus, T. L.; Elbert, S. T. *Quantum chemistry program exchange (QCPE)* **1990**, *10*, 52. (b) Schmidt, M. W.; Baldridge, K. K.; Boatz, J. A.; Elbert, S. T.; Gordon, M. S.; Jensen, J. H.; Koseki, S.; Natsunaga, M.; Ngueyen, K. A.; Su, S.; Windus, T. L. *J. Comput. Chem.* **1993**, *14*, 1347−1363.

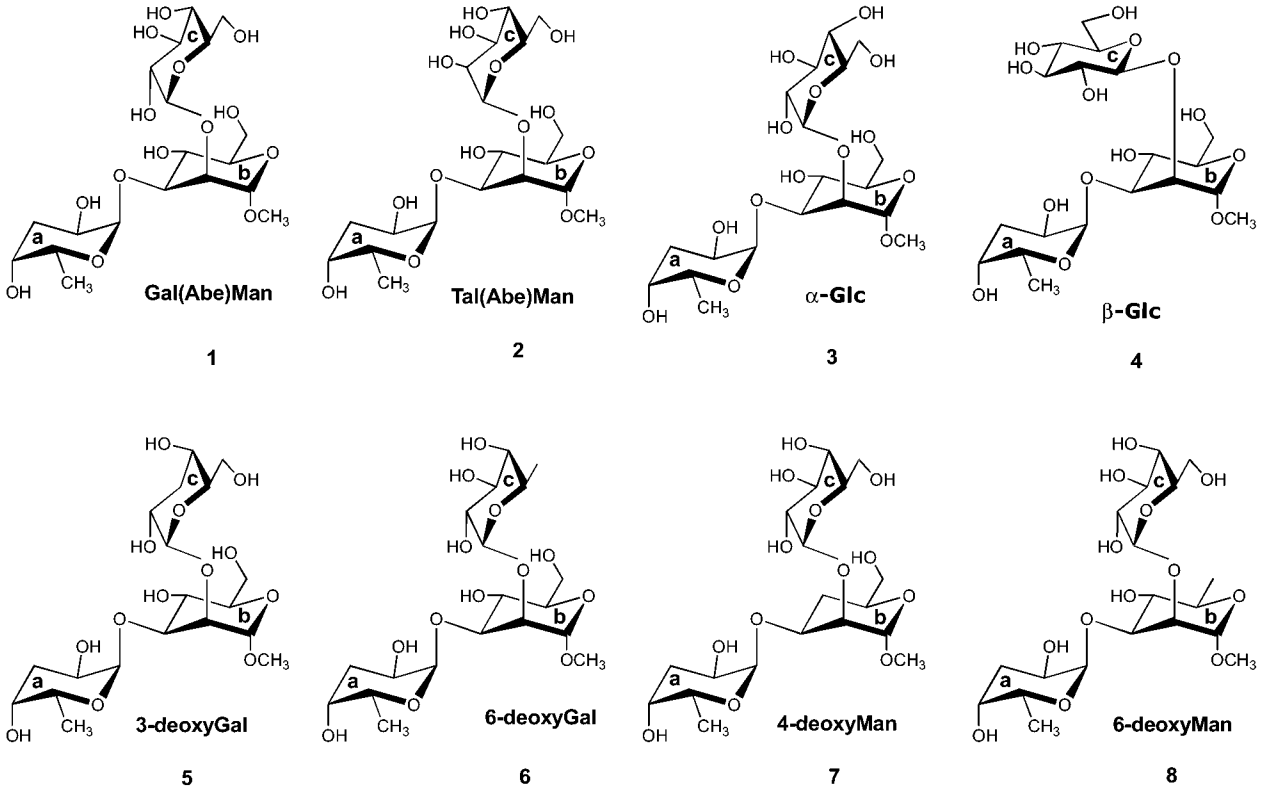

Figure 2. Structure of trisaccharide ligands.

conformational search option in HyperChem. Three hundred initial structures were generated by randomly varying four dihedral angles in the histidine molecule (NC_{ring}-CH, CH−NH, HN−CO, HO−CO). Each conformer was then subjected to full geometry optimization using the AM1 method. The lowest-energy structure identified from the search was then further optimized at the HF level, and the vibrational frequencies were calculated. The optimized structures (HF/6-31G**) of imidazole (the side chain of histidine) and a single conformer of β-galactose (Gal) were used to construct a starting structure for the hydrogen-bonded complex of imidazole and Gal (where the NH group of imidazole served as the hydrogen bond donor and the C-3 OH group acted as the hydrogen bond acceptor). Geometry optimization was performed on a single conformation of the complex. The zero-point energy of imidazole, Gal, and the complex were determined from the calculated vibrational frequencies. The optimized structures and corresponding energies and vibrational frequencies are included in Supporting Information.

Results and Discussion

For gas-phase dissociation studies to provide useful insight into the nature and strength of intrinsic protein−ligand interactions the following criteria must be satisfied. First, some or all of the solution-specific interactions must be retained throughout the electrospray and desolvation processes. If structural changes occur in the binding region, it is necessary to deconvolute the solution specific interactions from those that originate in the gas phase. Second, the energetic stability of the complexes must reflect the strength of the gas-phase interactions, with minimal contribution from Coulombic repulsion and conformational changes that accompany the loss of the ligand. Below, we discuss both criteria and the extent to which they are satisfied in the present system.

Influence of Charge on the Dissociation Pathways, Kinetics and Energetics. A single complex, (scFv + **2**), was chosen as a model system for investigating the effect of the number and nature of the charges on the decomposition pathways, kinetics, and energetics. Due to its greater availability at the time, the trisaccharide **2** was chosen instead of the native trisaccharide **1**. **2** differs structurally from **1** in the axial position of the 2-OH of residue c (see Figure 2).

NanoES of scFv−Tal[Abe]Man Complex. NanoES of an aqueous solution containing $\sim 10^{-5}$ M scFv and $\sim 10^{-5}$ M **2** resulted in similar yields of $scFv^{n+}$ ions and the 1:1 complex with **2**. At a solution flow rate of ~100 nL/min (controlled by the dimensions of the nanoES tip), $scFv^{n+}$ and $(scFv + \mathbf{2})^{n+}$ ions were observed with charge states of $n = 9$ to 11. Abundant protonated ions were observed, that is $(scFv + \mathbf{2} + n\mathrm{H})^{n+}$, as well as ions containing one or more alkali metal ions (M^+), that is, $(scFv + \mathbf{2} + (n - p)\mathrm{H} + p\mathrm{M})^{n+}$ (Figure 3a). The spectral resolution was sufficient to identify the attachment of up to two Na^+ ions and at least one K^+ ion. At much lower solution flow rates, 5−10 nL/min, higher charge state ions were observed, $n = 11-13$. Interestingly, under these conditions the ions were found to be almost exclusively protonated, with virtually no M^+ attachment (Figure 3b). There was no evidence, under either flow regime or over a range of sampling conditions, for the retention of the structural water molecules observed in the crystal structure. Under both flow regimes, a small amount of the 1:2 complex, $(scFv + 2(\mathbf{2}))^{n+}$, was also observed. The scFv is known to bind specifically to a single oligosaccharide ligand in solution. Therefore, any 1:2 complex must originate from nonspecific binding during the nanoES process. To verify that nonspecific binding did not contribute appreciably to the 1:1

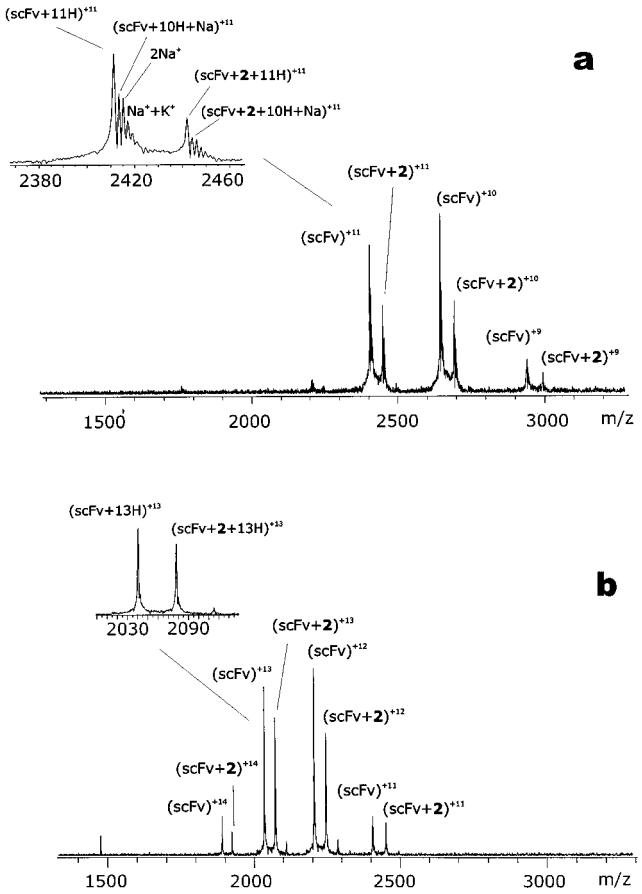

Figure 3. NanoES spectra of aqueous solutions scFv (10 μM) and **2** (10 μM) obtained at flow rates of (a) ~100 nL/min and (b) ~5 nL/min.

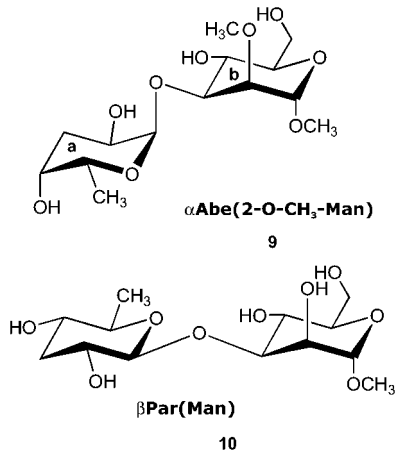

Figure 4. Structure of disaccharide ligands.

complex in the gas phase, nanoES was performed on a solution containing a related but stereochemically distinct disaccharide βPar(Man) (**10**, Figure 4) which does not bind specifically to the scFv in solution. As expected, very little (scFv + **10**)$^{n+}$ complex was observed in the mass spectrum (the abundance of 1:1 complex was ~5% that of the unbound scFv ions).

The relationship between the solution flow rate, charge state, and the abundance of metal ion adducts is not understood. The nanoES droplets may experience a small decrease in pH, due to the oxidation of water at the Pt electrode, at the lower flow rates.[27] Partial denaturation of the protein, resulting from the decrease in pH, would lead to an increase in the charge states

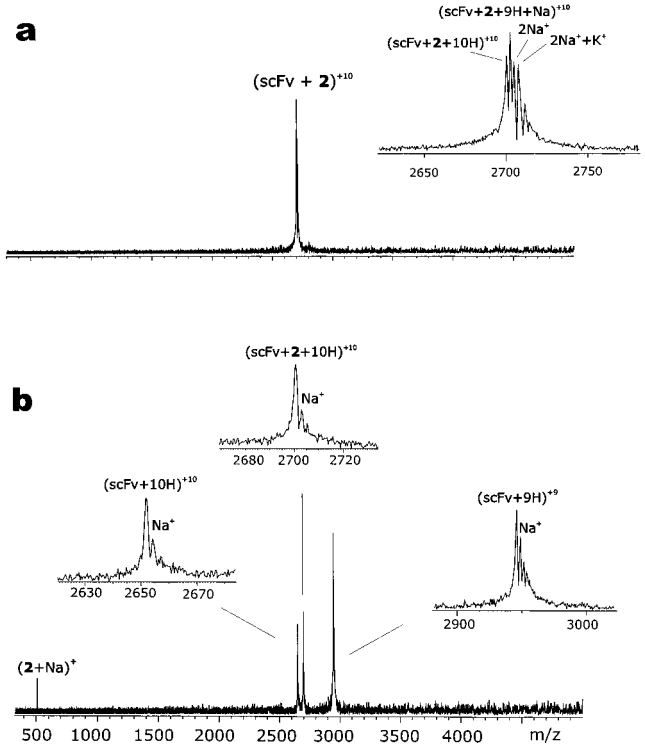

Figure 5. Blackbody infrared radiative dissociation spectra of the (scFv + **2**)$^{10+}$ complex: (a) 0 s, 125 °C, (b) 100 s, 125 °C.

observed for the gaseous ion.[28] However, any decrease in the pH would have to be quite modest since the solution was buffered at pH 6.7 with 1 mM $CH_3CO_2NH_4$. Furthermore, the association constant for the complex is very sensitive to pH, with a complete loss of binding below pH ~5.[21] Finally, the stability of the +11 complex generated under both flow regimes was identical, suggesting that the solution structures of the complexes (at least in the binding region) were also identical. The concomitant suppression of the metal ion adducts at lower flow rates, and presumably lower pH, may simply reflect the increased relative concentration of the protonating agents (NH_4^+, H_3O^+) compared with the alkali metal ions which are present in the solution as impurities (e.g., $[Na^+] \approx 10\ \mu M$).

b. Dissociation of (scFv + 2)$^{n+}$. Pathways and Kinetics. It was not possible to isolate only the protonated complex in the ion cell. Therefore, BIRD was performed simultaneously on the protonated and alkali metal ion (M^+)-containing complexes at a given charge state. A typical BIRD spectrum, obtained for the +10 charge state at 398 K, is shown in Figure 5. Depending on the nature of the charging agents, decomposition of the complex proceeded by loss of either neutral or charged ligand (eqs 2, 3). The fully protonated complex, (scFv + **2** + nH)$^{n+}$, decomposed exclusively by loss of neutral **2** (eq 2). There was no evidence of the **2**·H$^+$ ion or any of its fragment ions in the spectra over the temperature range investigated. Small amounts of the (scFv + ($n - p$)H + pM)$^{n+}$ ions were also observed, corresponding to the loss of neutral **2** from the (scFv + **2** + ($n - p$)H + pM)$^{n+}$ complexes (eq 3a). However, the kinetically dominant dissociation pathway for the M^+-containing complexes

(27) (a) Van Berkel, G. J.; Asano, K. G.; Schnier, P. D. *J. Am. Mass Spectrom* **2001**, *12*, 853−862.(b) Konermann, L.; Silva, E. A.; Sogbein, O. F. *Anal. Chem*. **2001**, *73*, 4836−4844.
(28) Konermann, L.; Douglas, D. J. *Biochemistry* **1997**, *36*, 12296−12302.

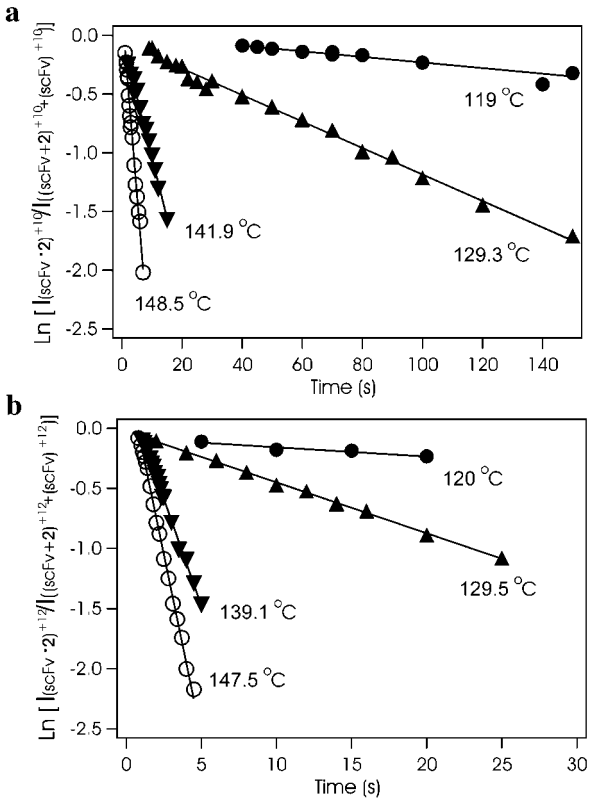

Figure 6. Kinetic data for the loss of **2** from (a) $(scFv + \mathbf{2} + 10H)^{10+}$ and (b) $(scFv + \mathbf{2} + 12H)^{12+}$, fit to first-order kinetics at the temperatures indicated.

was the loss of charged ligand, $\mathbf{2}\cdot M^+$ (eq 3b).

$$(scFv + \mathbf{2} + nH)^{n+} \rightarrow (scFv + nH)^{n+} + \mathbf{2} \quad (2)$$

$$(scFv + \mathbf{2} + (n-p)H + pM)^{n+} \rightarrow (scFv + (n-p)H + pM)^{n+} + \mathbf{2} \quad (3a)$$

$$\rightarrow (scFv + (n-p)H + (p-1)M)^{(n-1)+} + \mathbf{2}\cdot M^+ \quad (3b)$$

The rate constants for the loss of **2** from the protonated complexes were determined from a linear least-squares fit of plots of the natural logarithm of the relative abundance of the complex (R_{scFvL}) versus reaction time. The value of R_{scFvL} was determined from the expression:

$$R_{scFvL} = I_{scFv\mathbf{2}}/(I_{scFv\mathbf{2}} + I_{scFv}) \quad (4)$$

where I_{scFv2} and I_{scFv} are the measured intensities for the protonated $(scFv + \mathbf{2})^{n+}$ and $scFv^{n+}$ ions, respectively. Kinetic plots obtained for the $(scFv + \mathbf{2} + 10H)^{+10}$ and $(scFv + \mathbf{2} + 12H)^{+12}$ ions, at four temperatures, are shown in Figure 6. The plots were found to exhibit good linearity over the reaction extent investigated, with near zero intercepts. Plots of similar quality were obtained for all charge states. The dissociation kinetics are consistent with the unimolecular decomposition of a single reactant. This suggests that, at a given charge state, the structure in the binding region was similar for all of the gaseous complex ions produced by nanoES. The linear kinetics also indicated that nonspecific association during the nanoES process did not contribute appreciably to the formation of the 1:1 complex ions.

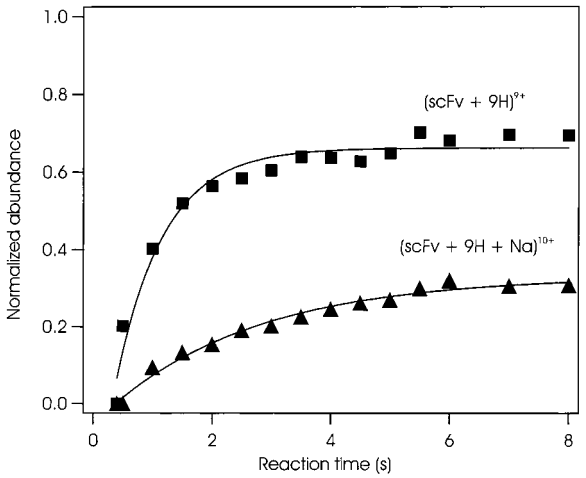

Figure 7. Normalized products ion appearance curves for $(scFv + 9H + Na)^{10+}$ and $(scFv + 9H)^{9+}$ produced by BIRD of $(scFv + \mathbf{2} + 9H + Na)^{10+}$. The solid lines represent single-exponential fits of the appearance curves.

The dissociation kinetics for the loss of **2** and $\mathbf{2}\cdot Na^+$ from the $(scFv + \mathbf{2} + (n-1)H + Na)^{n+}$ complexes, where $n = 10$ and 11, were also evaluated. From plots of the normalized abundance of the $(scFv + (n-1)H + Na)^{n+}$ and $(scFv + (n-1)H)^{(n-1)+}$ product ions versus reaction time (Figure 7), it can be seen that the dissociation channel leading to the formation of $(scFv + (n-1)H)^{(n-1)+}$ and $\mathbf{2}\cdot Na^+$ (eq 3b) did not contribute at long reaction times (reaction extent). On the other hand, production of the $(scFv + (n-1)H + Na)^{n+}$ ion (eq 3a) occurred over the entire extent of reaction. This behavior is not consistent with the unimolecular decomposition of a single parent ion via two parallel pathways. Instead, the kinetics suggest that the $(scFv + \mathbf{2} + (n-1)H + Na)^{n+}$ parent ion actually consisted of two (at least) distinct complexes, which lose either **2** or $\mathbf{2}\cdot Na^+$, but not both (eq 5a, b). The complex that loses the neutral ligand is identified with the subcripts *n*, while the complex that loses charged ligand is labeled with *c*.

$$(scFv + \mathbf{2} + (n-1)H + Na)_n^{n+} \rightarrow (scFv + (n-1)H + Na)^{n+} + \mathbf{2} \quad (5a)$$

$$(scFv + \mathbf{2} + (n-1)H + Na)_c^{n+} \rightarrow (scFv + (n-1)H)^{(n-1)+} + \mathbf{2}\cdot Na^+ \quad (5b)$$

The overall (observed) dissociation kinetics would reflect the fraction of each complex and the corresponding dissociation rate constants. The rate constants for the loss of neutral **2** (k_n) and loss of $\mathbf{2}\cdot Na^+$ (k_c) were determined by fitting plots of the normalized abundance of the two product ions to a single-exponential function (eq 6a or b):

$$\ln[1 - (I_{scFv}{}^{n+}/(1 - R_c)\,(I_{scFv\mathbf{2}}{}^{n+} + I_{scFv}{}^{(n-1)+} + I_{scFv}{}^{n+}))] = -k_n t \quad (6a)$$

$$\ln[1 - (I_{scFv}{}^{(n-1)+}/R_c\,(I_{scFv\mathbf{2}}{}^{n+} + I_{scFv}{}^{(n-1)+} + I_{scFv}{}^{n+}))] = -k_c t \quad (6b)$$

where $I_{scFv\mathbf{2}}{}^{n+}$, $I_{scFv}{}^{(n-1)+}$ and $I_{scFv}{}^{n+}$ are the measured intensities of the complex and the two products, normalized for charge. R_c is the fractional abundance, normalized for charge, of the two complexes (*n* and *c*). The value of R_c was determined from

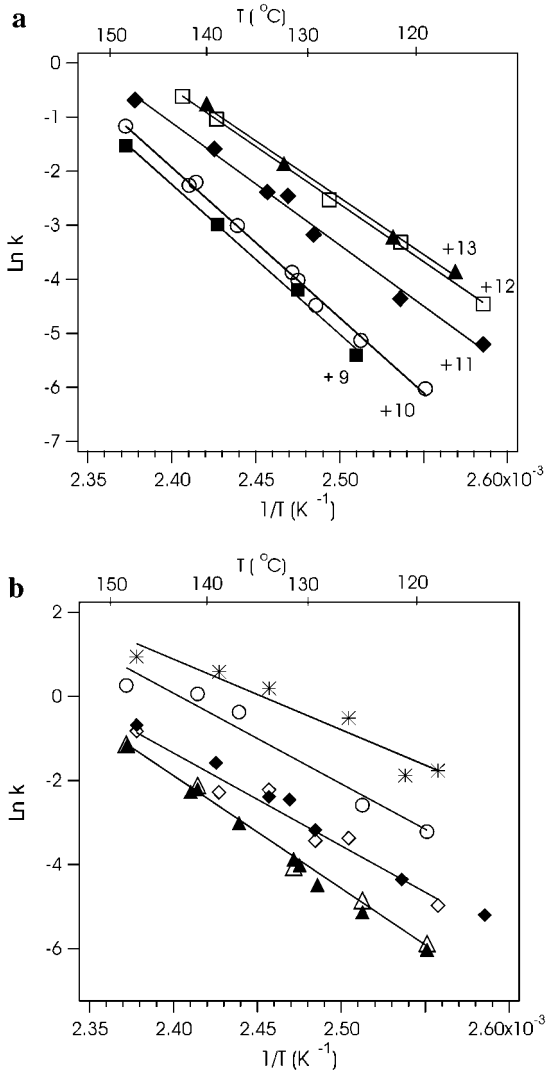

Figure 8. (a) Arrhenius plots for the loss of **2** from (scFv + **2** + *n*H)$^{n+}$: ■ (n = 9), ○ (10), ◆ (11), □ (12), ▲ (13), (b) Arrhenius plots for the loss of **2** and **2**·Na$^+$ from (scFv + **2** + 9H + Na)$^{10+}$ and (scFv + Tal[Abe]Man + 10H + Na)$^{11+}$: ▲ (loss of **2** from +10), ◆ (loss of **2** from +11); ○ (loss of **2**·Na$^+$ from +10) ∗ (loss of **2**·Na$^+$ from +11).

the abundance of the scFv^{n+} and scFv$^{(n-1)+}$ ions measured at relatively long reaction extents:

$$R_c = I^{\max}{}_{\mathrm{scFv}}{}^{(n-1)+}/[I^{\max}{}_{\mathrm{scFv}}{}^{(n-1)+} + (I^{\max}{}_{\mathrm{scFv}}{}^{n+}\,(n-1)/n)] \quad (7)$$

The magnitude of R_c varied somewhat between experiments. In general, 50−70% of the ions underwent loss of **2**·Na$^+$.

c. Arrhenius Parameters and Dissociation Mechanisms. Arrhenius plots were constructed from the temperature-dependent rate constants measured for the loss of **2** from (scFv + **2** + *n*H)$^{n+}$ and the loss of **2** and **2**·Na$^+$ from (scFv + **2** + (n − 1)H + Na)$^{n+}$ (Figure 8, a, b). Over the temperature range investigated, the kinetic stability of the protonated complex decreased with increasing charge state. The rate constants for the loss of **2** from (scFv + **2** + (n − 1)H + Na)$^{n+}$ were similar to those measured for the protonated complex, while the rate constants for the loss of **2**·Na$^+$ were found to be larger than for the loss of neutral **2**. The dissociation activation energy, E_a, was determined from the slope of a linear least-squares fit of the

Table 1. Arrhenius Parameters Measured for the Loss of Tal[Abe]Man (**2**) and **2**·Na$^+$ from (scFv + **2** + *n*NH + *p*Na)$^{(n+p)+}$

n, p	products	E_a (kcal/mol)	A (s^{-1})
9, 0	**2**/(scFv +*n*H)$^{n+}$	55.0 ± 2.4	$10^{27.9\pm1.3}$
10, 0	**2**/(scFv +*n*H)$^{n+}$	55.3 ± 1.2	$10^{28.2\pm0.7}$
11, 0	**2**/(scFv +*n*H)$^{n+}$	45.0 ± 1.9	$10^{23.1\pm1.0}$
12, 0	**2**/(scFv +*n*H)$^{n+}$	42.3 ± 0.7	$10^{22.0\pm0.4}$
13, 0	**2**/(scFv +*n*H)$^{n+}$	41.7 ± 1.7	$10^{21.8\pm0.9}$
9, 1	**2**/(scFv + *n*H + *p*Na)$^{(n+p)+}$	53.4 ± 2.4	$10^{27.2\pm1.3}$
	2·Na$^+$/(scFv +*n*H)$^{n+}$	42.0 ± 7.0	$10^{22.1\pm3.8}$
10, 1	**2**/(scFv + *n*H + *p*Na)$^{(n+p)+}$	44.0 ± 4.6	$10^{22.5\pm2.5}$
	2·Na$^+$/(scFv +*n*H)$^{n+}$	33.4 ± 4.6	$10^{17.9\pm2.5}$

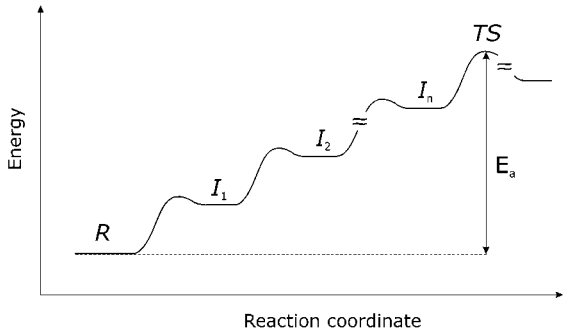

Figure 9. Hypothetical "staircase" reaction coordinate for the loss of the ligand from a protein−ligand complex by the sequential cleavage of the intermolecular hydrogen bonds.

Arrhenius plot and the preexponential factor (A) was determined from the y-intercept. The measured Arrhenius parameters are listed in Table 1. The trend of decreased kinetic stability with increasing charge state (for n = 10−13) mirrors the trend in energetic stability: E_a = 55.0 (+9), 55.3 (+10), 45.0 (+11), 42.3 (+12), and 41.7 kcal/mol (+13). The A-factors were also found to decrease with increasing charge state (n = 10−13): $10^{27.9}$ (+9), $10^{28.2}$ (+10), $10^{23.1}$ (+11), $10^{22.0}$ (+12), and $10^{21.8}$ s^{-1} (+13). The Arrhenius parameters for the loss of **2** and **2**·Na$^+$ from the monosodiated complex were: 53.4 ± 2.4 kcal/mol, $10^{27.2\pm1.3}$ s^{-1} and 42.0 ± 7.0, $10^{22.1\pm3.8}$ (+10); 44.0 ± 4.6, $10^{22.5\pm2.5}$ and 33.4 ± 4.6, $10^{17.9\pm2.5}$ (+11), respectively.

Loss of the oligosaccharide ligand from the complex requires the cleavage of all of the stabilizing intermolecular interactions. As discussed above, it is assumed that hydrogen bonding accounts for the bulk of the energetic stability of the complex in the gas phase. The simplest mechanism to represent this dissociation process is a "staircase mechanism" wherein the intermolecular hydrogen bonds are cleaved sequentially, with the transition state (*TS*) corresponding to the cleavage of the last remaining interaction. A simplistic two-dimensional diagram for such a process is shown in Figure 9. Of course, the use of a two-dimensional reaction coordinate to represent what is a complicated energy surface (landscape) is a gross oversimplification but is used here for conceptual purposes. According to this mechanism, a series of intermediate structures (*I*), which differ by the number of intact hydrogen bonds, lie along the reaction coordinate between the reactant (*R)* and the *TS*. If bond cleavage occurs without significant conformational changes in the protein or the ligand, and without intramolecular resolvation, then the difference in energy between successive intermediate structures (i.e., I_{n-1} and I_n), should reflect the energy of the hydrogen bond. According to transition-state theory, the rate of the reaction depends only on the free energy of activation

($\Delta G^{\ddagger} = -RT \ln K^{\ddagger}$, where $K^{\ddagger}$ is the equilibrium constant governing the interconversion of *TS* and *R*) at the reaction temperature:

$$k = k_B T/h \exp(-\Delta G^{\ddagger}/RT) = k_B T/h \exp(\Delta S^{\ddagger}/R) \exp(-\Delta H^{\ddagger}/RT) \quad (8)$$

Therefore, the presence of many intermediate structures, which lie along the reaction surface and are higher in energy than *R*, should not influence the rate of decomposition. In the absence of extensive intramolecular solvation of groups originally involved in intermolecular interactions, the enthalpy of activation ($\Delta H^{\ddagger}$) will reflect the sum of all the individual binding energies in *R*. In this case, the magnitude of the dissociation E_a, which is approximately equal to $\Delta H^{\ddagger}$,[29] should provide a reliable measure of the strength of the stabilizing intermolecular interactions. Support for this very important assumption is provided in a proceeding section.

The E_a's measured for the different charge states ($n = 10-13$) indicate that the structure of the binding site and the nature and number of the stabilizing interactions are influenced by electrostatic repulsion. The decrease of ~10 kcal/mol with the addition of the 11th proton and a further 3 and 4 kcal/mol with the 12th and 13th protons, respectively, indicates a reduction or weakening of the intermolecular interactions with the addition of charge. Since the dissociation process involves the loss of a neutral molecule, the charge cannot exert a direct electrostatic influence on the dissociation energy. Instead, the charge must have influenced the structure of the binding region in the complex. Ion mobility measurements, performed on gaseous protein ions have shown that increasing the charge state results in Coulombic repulsion-induced unfolding (and expansion) of the protein ions.[4] It is, therefore, likely that the binding region of the complex was influenced by the electrostatic-induced unfolding, resulting in a reduction in stability at higher charge states. From the present results it was not possible to determine the nature of the structural differences. However, we are currently investigating the relative stability of all the trisaccharide analogues, over the range of accessible charge states, as well as a number of scFv mutants, to assess how the binding region of the protein changes with charge state. In contrast to the trend in E_a observed for $n = 10-13$, similar E_a's were obtained for $n = 9$ and 10. This suggests that the structure of the complex at the two charge states, at least in the binding site, was similar. This result further suggests that, for $n < 11$, the Coulombic repulsion effects may be negligible in terms of the intermolecular interactions, and that the E_a's are independent of *n*. To test this assumption it would be necessary to measure the E_a for the +8 and, if possible, lower charge states. Unfortunately, the abundance of these lower charge ions was too low to perform these measurements.

While it may be tempting to speculate on the number and nature of the intermolecular hydrogen bonds based on the E_a's determined for the different charge states, it is impossible to extract specific structural information. The strength of the hydrogen bonds (and any other intermolecular interactions) which contributes to the stability of the complex will reflect the nature of donor and acceptor groups, as well as possible conformational (steric) constraints. As described below, significant variation in the energetic contribution of individual oligosaccharide OH groups has been identified, presumably reflecting one or both of the above factors. Therefore, it is ill advised to try to assess the number of hydrogen bonds, based on some average hydrogen bond energy. A further difficulty in assessing the present energetic data is the absence of comparable data for other protein−ligand complexes.

Dissociation of the $(\text{scFv} + \mathbf{2})^{n+}$ complex is expected to proceed with a very loose transition state. This was confirmed by the large *A*-factors, which were found to increase with decreasing charge state. The *A*-factors measured for the +12 and +13 complex are comparable to values reported for the dissociation of DNA duplex anions composed of complementary 7-mers, $\sim 10^{20}$ s^{-1}.[18] The *A*-factors determined for the +11 to +9 charge states are even larger, $> 10^{23}$ s^{-1}. Comparable *A*-factors have only ever been reported for the loss of protein subunits from multiprotein assemblies.[19,20]

To facilitate the interpretation of the *A*-factors it is convenient to convert them into their corresponding entropy of activation ($\Delta S^{\ddagger}$) using the following expression:[29]

$$A = (ek_B T/h) \exp(\Delta S^{\ddagger}/R) \quad (9)$$

The $\Delta S^{\ddagger}$ values calculated at 400 K are: 67 (+9), 67 (+10), 44 (+11), 39 (+12), and 38 cal/mol K (+13). The release of internal rotations, initially frozen out in the *R* by a network of hydrogen bonds, likely accounts for the majority of the increase in entropy of the *TS* and, consequently, in $\Delta S^{\ddagger}$. The magnitude of $\Delta S^{\ddagger}$ will reflect the number and nature of the hydrogen bond donor and acceptor groups in the protein and ligand. Although it is not possible from the present work to identify the amino acids that interact with the ligand, the internal rotations of residues located in the binding pocket, as shown by the crystal structure, could account for a significant portion of the $\Delta S^{\ddagger}$. For example, the side chains of the histidine and tryptophan residues located within the binding pocket act as hydrogen bond donors to the trisaccharide (see Figure 1). Hydrogen bonding to the NH group of imidazole or indole rings will stiffen the vibrational modes corresponding to rotation of the ring and the entire side chain and result in a decrease in the entropy of the complex. While it is impossible to determine the actual contribution of particular rotational modes, upper limits for particular modes can be estimated from their vibrational frequencies determined from theoretical calculations. For example, from a vibrational analysis performed at the HF/6-31G** level of theory, the vibrational frequency corresponding to the internal rotation of the imidazole ring in histidine was calculated to be ~33 cm^{-1}. The freezing out of this mode due to hydrogen bonding of the side chain to the oligosaccharide would cost the complex ~6 cal/mol K in entropy at 400 K (treating this vibration as a harmonic oscillator).[30] Consequently, release of this rotation during the loss of the ligand could contribute as much as 6 cal/mol K to $\Delta S^{\ddagger}$. An even greater contribution would result from freezing out the rotation of the indole ring, which has a larger moment of inertia than imidazole. Other amino acid side chains, as well as amide groups may participate in stabilizing the complex in the gas phase and contribute to entropy of activation. The entropy of internal rotation for all of the amino acid side chains has been estimated at 298 K by

(29) Atkins, P. W. *Physical Chemistry*; Freeman: New York, 1998.

(30) Benson, S. W. *Thermochemical Kinetics*; Wiley: New York, 1976.

Doig.[31] Entropies as large as 10 cal/mol K per rotational mode were reported. These computational results clearly indicate that the release of restricted internal rotations could easily account for the large $\Delta S^{\ddagger}$ values measured in the present work.

The internal rotations associated with the oligosaccharide ligand may also contribute significantly to $\Delta S^{\ddagger}$. The hydrogen bond network is expected to restrict the rotational motion of some of the hydroxyl groups as well as the rotation of the individual monosaccharides about the glycosidic bonds. The entropy for the hindered rotation of the hydroxyl group in CH_3-OH has been calculated to be 7.3 cal/mol K (at 298 K).[32] This value should correspond to the upper limit to the entropy associated with the internal rotation of individual oligosaccharide OH groups (at the same temperature), which may be hindered by larger energy barriers. Rotation of the monosaccharides about the glycosidic bonds is also expected to contribute to the entropy, although the magnitude of this contribution has not, to our knowledge, been determined in the gas phase.

Arrhenius parameters for the loss of neutral **2** from the (scFv + **2** + $(n - 1)$H + Na)$^{n+}$ complexes were similar to the parameters measured for the loss of **2** from the protonated complexes. It is believed that the propensity for the complex to lose a neutral compared with a charged ligand depends on the location of the sodium ion. If the Na^+ is bound remote from the sugar, then the ligand is lost as a neutral (eq 5a), while is if it is bound directly to **2** it is lost as **2**·Na^+. The similarity in the Arrhenius parameters measured for the loss of **2** from the protonated and monosodiated complexes suggests that the actual location of the Na^+, as long as it is not bound to the ligand, had no significant effect on the reactivity. For a given charge state, the E_a for the loss of **2**·Na^+ was ~11 kcal/mol lower than for the loss of neutral **2** (see Table 1). The lower E_a is attributed to the competitive binding of Na^+ and scFv with **2**. Oligosaccharides are known to have high sodium ion affinities in the gas phase. Using the kinetic method, Wesdemiotis and coworkers recently reported sodium ion affinities of 47−48 kcal/mol for several disaccharides.[33] The affinities were attributed to the ability of the disaccharides to solvate Na^+ through multiple (as many as four) interactions with the ether and hydroxyl group oxygens. Trisaccharides should be able to solvate Na^+ as well or better than disaccharides and the sodium ion affinities of the trisaccharides should be similar or greater. Therefore, it is likely that the solvation of Na^+ by **2** reduces the number of OH groups hydrogen-bonded to the scFv. Electrostatic repulsion between **2**·Na^+ and the rest of the complex was also expected to influence the energy barrier to dissociation. However, based on the experimental data, this was not the case. One possible explanation for this result is the separation of the Na^+ ion and the other charges is sufficiently large that the electrostatic repulsion is small and its effect on E_a cannot be seen within the precision of our data.

Stability of the (scFv + tri +10H)$^{+10}$ Complexes. The aforementioned results revealed that the charge state of the (scFv + **2** + nH)$^{n+}$ complex, at least for $n = 10-13$, influenced the decomposition kinetics and energetics. Within this range, the absolute and, possibly, the relative binding energies measured for the trisaccharide ligands (**1**−**8**) will depend on the charge state. The similarity in the energetics for the +9 and +10 charge states suggests that electrostatic effects on the dissociation energies are negligible for $n \leq 10$. Therefore the +10 charge state was chosen for this first comparative study of the kinetic and energetic stability of the trisaccharide ligands. Shown in Figure 10 are the Arrhenius plots obtained for the (scFv + **tri** +10H)$^{+10}$ complexes composed of **1** and the seven structurally related trisaccharide analogues (**2**−**8**). The Arrhenius parameters determined from these plots are listed in Table 2, along with the association enthalpy and entropy changes measured in solution.[21]

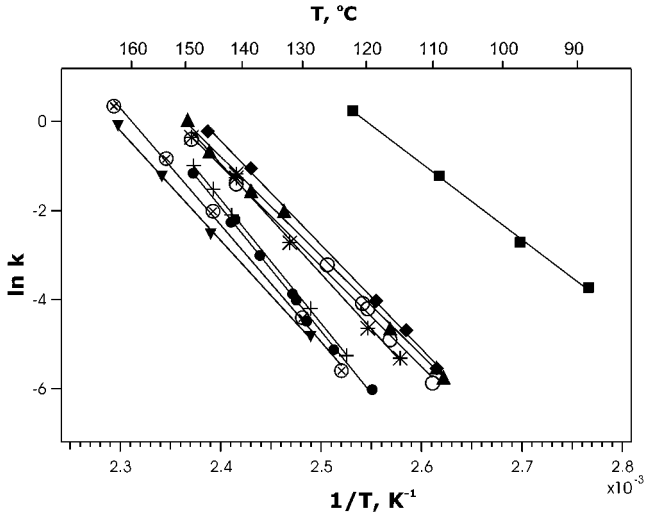

Figure 10. Arrhenius plots for the loss of the trisaccharide (**tri**) and disaccharide (**di**) ligands from (scFv + **tri** + 10H)$^{10+}$ and (scFv + **di** + 10H)$^{10+}$: + (trisaccharide **1**), ● (**2**), ⊗ (**3**), ▼ (**4**), ▲ (**5**), ○ (**6**), ∗ (**7**), ◆ (**8**), ■ (disaccharide **9**).

Table 2. Arrhenius Activation Parameters for the Loss of Neutral Trisaccharide (**tri**) from (scFv + 10H + **tri**)$^{+10}$

tri	E_a (kcal/mol)	A (s^{-1})	$-\Delta H^{\circ}_{assoc}$[a] (kcal/mol)	$-\Delta S^{\circ}_{assoc}$[a] (cal/mol K)
Galα[Abe]Man (**1**)	55.2 ± 0.6	$10^{28.3\pm0.3}$	4.9 ± 0.1	−8.0 ± 0.5
Talα[Abe]Man (**2**)	55.3 ± 1.2	$10^{28.2\pm0.7}$	9.1 ± 0.4[b]	7.5 ± 0.8[b]
Glcα[Abe]Man (**3**)	52.2 ± 1.3	$10^{26.4\pm0.7}$	9.0 ± 0.3	6.7 ± 0.9
Glcβ[Abe]Man (**4**)	48.9 ± 1.2	$10^{24.6\pm0.6}$	2.9 ± 0.8	−10.8 ± 2.9
(3-deoxy-Gal)[Abe]Man (**5**)	44.2 ± 1.0	$10^{22.9\pm0.5}$	7.9 ± 0.5	3.8 ± 1.8
(6-deoxy-Gal)[Abe]Man (**6**)	44.7 ± 1.2	$10^{23.1\pm0.7}$	4.9 ± 0.4	−6.3 ± 1.8
Gal[Abe](4-deoxy-Man) (**7**)	49.1 ± 1.3	$10^{25.4\pm1.3}$	6.6 ± 0.9	0.6 ± 3.1
Gal[Abe](6-deoxy-Man) (**8**)	46.4 ± 0.9	$10^{24.2\pm0.7}$	6.3 ± 0.3	−1.4 ± 1.0

[a] Association enthalpy and entropy changes measured in solution were taken from ref 21. [b] Unpublished data.

All four of the complexes composed of the monodeoxy trisaccharides (**5**−**8**) exhibited lower kinetic and energetic stability compared with **1**. Compounds **5**−**8** are a set of monodeoxy congeners (congeners are structural analogues of the epitope) modified in the mannose and galactose residues (i.e residues b and c). The E_a's measured for the monodeoxy ligands decreased by 11.0 for (**5**), 10.5 (**6**), 6.1 (**7**) and 8.8 kcal/mol for (**8**), compared to **1**. The reduction in E_a upon removal of the OH groups at the Gal C-3 and 6 and Man C-4 and 6 positions is compelling evidence that these groups interact with the scFv and stabilize the gaseous (scFv + **1** +10H)$^{+10}$ complex. In addition to providing a method for identifying the trisaccharide hydroxyl groups participating in intermolecular interactions, the energetic measurements also provided a quantitative measure of the interaction energy. Assuming that there is little or no reverse activation energy barrier for the dissociation of these

(31) Doig, A. J. *Biophys. Chem.* **1996**, *61*, 131−141.
(32) East, A. L. L.; Radom, L. *J. Chem. Phys.* **1997**, *106*, 16, 6655−6674.
(33) Cerda, B. A.; Wesdemiotis, C. *Int. J. Mass Spectrom. Ion Processes* **1999**, *189*, 189−204.

interactions, the present measurements provide insight into the binding enthalpy of specific OH groups to the protein. However, structural interpretation of the results is hindered by the fact that each OH group can, in principle, participate in several hydrogen bonds. To our knowledge, there have been no previous reported experimental or theoretical determinations of the intrinsic strength of protein−oligosaccharide hydrogen bonds. To this end, we have begun to calculate the strength of hydrogen bonds formed between the monosaccharides and the protein backbone and side chains. Using a 6-31G** basis set and correcting for zero-point energy, we have calculated the energy of minimized structure of imidazole, Gal and one conformation of the imidazole−Gal complex, formed by a hydrogen bond between the NH group of the imidazole ring and the C-3 OH group of Gal. From the calculated energies, an interaction energy of 6.3 kcal/mol was obtained.[34] Ornstein and co-workers[35] have reported a hydrogen bond energy, calculated at the MP2−FC/6-31++(2d,2p) level of theory, of 7.9 kcal/mol for the related water−imidazole complex. In this same work, the authors reported energies of 2 and 3 kcal/mol for hydrogen bonds between water and the C_δ and C_ϵ hydrogen of imidazole, respectively. These latter results highlight the fact that hydrogen bonds between the oligosaccharide and weakly acidic amino acid groups, may also contribute to the stability of the complex. On the basis of these computational results and the present experimental results, it seems likely that the two C-6 OH groups of **1** (residues b and c) participate in multiple H-bonds (i.e., act as both donor and acceptor). This is also likely the case for the Gal C-3 OH, although one cannot rule out a single, strong hydrogen bond. For Man C-4 OH, however, the energetic data are suggestive of a single interaction.

Replacement of the αGal monosaccharide in **1** (residue c) by αTal (**2**) and αGlc (**3**) provided additional insights into the nature of the scFv−**1** interactions. Gal and Tal are C-2 epimers (two sugars which are different only in the configuration around one carbon atom), while Gal and Glc are C-4 epimers. Replacement of αGal with αTal resulted in a small, 0.1 kcal/mol, increase in E_a. This result suggests that the C-2 OH group does not contribute to the stability the complex. This result is consistent with the Fab-**1** crystal structure in which the C-2 OH group participates in an intramolecular hydrogen bond with the C-2 OH of Abe. It could be argued, however, that this result is also consistent with both C-2 epimers being able to interact with the scFv, although perhaps with different amino acids. However, as described below, this explanation is not consistent with results obtained for the disaccharide Abe(2-O−CH_3-Man) (**9**). Replacement of αGal by αGlc resulted in a decrease of 3.0 kcal/mol in E_a. This suggests that the C-4 OH does contribute, albeit weakly, to the stability of the complex. As expected, replacement of αGal with βGlc (**4**) resulted in a significant decrease, 6.4 kcal/mol, in stability due to the altered anomeric configuration. It is perhaps surprising that a larger decrease in E_a was not observed. This result suggests that, at least the periphery of the binding region of the protein may be quite flexible and able to accommodate conformational changes in the ligand. Interestingly, the lower E_a's of **3** and **4**, compared to that from **1**, do not coincide with a decrease in kinetic stability (over the temperature range studied). In fact, the trend in kinetic stability was found to be opposite to that of the energetic stability, with the more weakly bound ligands being least reactive.

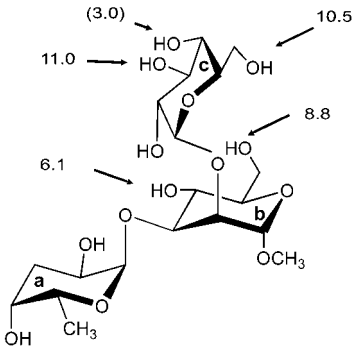

Figure 11. Map of hydrogen-bond interactions, originating from **1**, for the gaseous complex (scFv + **1** +10H)$^{+10}$.

An underlying assumption in the functional group replacement approach is that removal or modification of a single functional group does not alter (nature or strength) the remaining interactions or the ligand conformation. While it is impossible in the present work to ensure that modification of single OH groups (either orientation or deletion) did not disrupt the remaining interactions, indirect support for the validity of this approach was obtained from the dissociation E_a measured for the complex scFv with the disaccharide analogue, Abe(2-O−CH_3-Man) (**9**). The Arrhenius plot for the loss of **9** from the complex is shown in Figure 10. The Arrhenius parameters for the loss of the neutral **9** from the complex are 33.9 ± 0.9 kcal/mol (E_a) and $10^{18.9\pm0.5}$ s^{-1} (A), this E_a being 21.3 kcal/mol lower than for **1**. The decrease in E_a, upon removal of the monosaccharide Gal is, within the combined experimental error of the E_a measurements, equal to the sum of the interactions identified for the Gal residue (residue c) (i.e., 11.0 (6-OH) + 10.5 (3-OH) + 3.0 (4-OH) = 24.5 kcal/mol). This result strongly suggests that the structure and binding interactions for the AbeMan portion in (scFv + **1** + 10H)$^{+10}$ and (scFv + **9** +10H)$^{+10}$ are similar. This further supports the assumption that the structure of the complex in the gas phase is not sensitive to removal of single OH groups. A similar study of the stability of (scFv + Abe + 10H)$^{+10}$ was also attempted, but the solution binding constant for Abe is too small ($K_{assoc} = 1.4 \times 10^3$ M^{-1})[21] to generate sufficient gaseous complex to perform the BIRD experiments.

From the analysis of the differences in E_a described above, it was possible to construct a partial map of the oligosaccharide OH groups that participate in the intermolecular hydrogen bonds in the gaseous (scFv + **1** +10H)$^{+10}$ complex, see Figure 11. At least two hydroxyl groups per monosaccharide (Gal, Man and presumably Abe) are believed to bind to the scFv. However, the amino acids that act as the complementary hydrogen bond donor and acceptor groups cannot be identified from the present results. The amino acid bonding partners could be determined from dissociation experiments using scFv mutants, wherein amino acids located in the binding pocket have been altered. The sum of the energetic contributions of the oligosaccharide OH groups identified above account for 71% of the dissociation E_a measured for (scFv + **1** +10H)$^{+10}$. The Gal monosaccharide contributes approximately 24.5 kcal/mol, while Man contributes ~15 kcal/mol, toward the stability of the complex. The remaining 16 kcal/mol likely involves interactions with one or

(34) A single vibration with a small imaginary frequency was obtained from the harmonic vibrational analysis performed at the stationary point of the complex. The interaction energy of 6.3 kcal/mol, reported for the imidazole−Gal complex, was calculated using this lowest-energy structure.
(35) Ornstein, R. L.; Zheng, Y. J. *J. Biomol. Struct. Dyn.* **1997**, *14*, 657−665.

both of the Abe hydroxyl groups and possibly the OMe group of Man. Unfortunately, it was not possible to examine the contribution of the individual Abe OH groups through the use of monodeoxy analogues. Removal of either of the OH groups results in a profound loss of binding in solution,[21] making it difficult to form the gaseous complex by nanoES.

Comparison of the key intermolecular interactions originating from **1** in the gas phase with those in the crystal structure reveals that structural differences in the binding region exist in the gas and the condensed phases. In solution, the bulk of the association free energy (~60%) is attributed to interactions between the scFv and the Abe residue in **1**. The crystal structure indicates that both Abe hydroxyl groups participate in intermolecular hydrogen bonds, either directly to the scFv or indirectly, through a water molecule. The C-4 OH group of Man also interacts directly with the scFv. The C-6 OH groups of Man and Gal do not form key contacts with the protein surface and are believed exposed to solvent. In contrast, in the gas phase the Gal and Man C-6 OH groups account for more than one-third of the total dissociation E_a. The Gal C-3 and Man C-4 OH groups also contribute significantly. As described above, the remaining interactions likely involve the Abe and may bear some similarity with solution interactions, with the important exception of any interaction with water molecules in the interface. Therefore, groups that do not contribute significantly to the stability of the complex in solution are found to play a key role in stabilizing the complex in the gas phase. While these results may reflect the fact that the structure of the protein binding site may be significantly different in the gas phase, they may also be consistent with relatively subtle structural changes. For example, it was found that rotation of the C-6 OH groups in the energy minimized structure of the complex (minimized with the CVFF force field and a dielectric constant of 1.0) would allow these groups to participate in intermolecular hydrogen bonds with amino acid side chains. Further support for the retention of the structural integrity of the binding site has been obtained from preliminary BIRD experiments performed on (scFv + **2**) complexes composed of mutant scFv proteins.[36]

Replacement of His^{101H}, which is located within the binding pocket, with Gln resulted in a decrease in energetic stability by ~5 kcal/mol. No such decrease was observed for mutants involving similar modifications remote from the binding pocket. These results strongly suggest that, in the gas phase, **2** binds to amino acids that make up the binding site in solution. Since **1** exhibited dissociation kinetics and energetics similar to **2**, it is reasonable to conclude that **1** and indeed all the trisaccharide ligands are bound to the same region of the protein in the gas phase.

A comparison of the gas phase E_a's and the association enthalpies measured in solution (ΔH_{assoc}), reveals that there is no correlation between the binding energetics in the gas and condensed phases. Differences in relative stability of the trisaccharide analogues measured in the two phases can be explained by the structural differences described above, as well as by the influence of solvent reorganization in the aqueous phase. In solution, the binding site of the scFv is dominated by aromatic amino acids (His and Trp). The displacement of four water molecules from this relatively hydrophobic region to bulk solution, believed to accompany binding, contributes to the association thermochemistry, as does displacement of water molecules originally bound to the free oligosaccharide.[37] The significant influence of solvent reorganization at the ligand surface on binding can be seen from a comparison of the association thermodynamics measured for **1** and the monodeoxy analogues. The binding enthalpies ($-\Delta H_{assoc}$) measured for **5**, **7**, and **8** are larger than for **1**. However, the gain in enthalpy is more than offset by a loss in entropy (ΔS_{assoc}), leading to a net decrease in binding free energy ($-\Delta G_{assoc}$). The nature of this solvent effect is not fully understood, nor is it general. For example, all of the monodeoxy analogues of the native oligosaccahride of the lectin GS IV, exhibit a lower $-\Delta H_{assoc}$ than the native ligand.[1b] In the present system, the increased $-\Delta H_{assoc}$ (and concomitant decrease in ΔS_{assoc}) with deletion of a single OH group may reflect the fact that displacement of water from the OH group is enthalpically unfavorable. As a result, any enthalpy gained through binding of the oligosaccharide to the scFv is more than offset by the enthalpic cost of displacing the water. In the case of **5**, **6**, and **8**, the OH groups in question are not believed to form strong interactions with the protein but improve binding via a favorable entropy contribution resulting from the displacement of solvent. In the case of **6**, the association thermochemistry is similar to that of **1**. This result may reflect the fact that Gal C-6 OH, as shown by the crystal structure, is located at the periphery of the binding site and is the group most exposed to solvent.

Conclusions

The present work details the first application of a thermal activation technique (BIRD) and functional group replacement to map the nature and strength of the intermolecular interactions for a gaseous protein−ligand complex. Arrhenius E_a and *A*-factors were determined for the loss of structurally related trisaccharide ligands, including four monodeoxy trisaccharide congeners, bound noncovalently to the scFv of the monoclonal antibody (Se155-4). From the measured E_a's, a partial hydrogen-bond map was constructed for the gaseous $(scFv + \mathbf{1} + 10H)^{+10}$ complex. The map identifies the OH groups of **1** that hydrogen bond to the scFv and the strength of these interactions. The strength of the hydrogen bonds associated with particular OH groups ranged from 6 to 11 kcal/mol. This variability was attributed to differences in the amino acid bonding partners and conformational constraints. Comparison of the gas phase map with the crystal structure revealed that significant differences exist in the binding interactions in the gas and condensed phases. The OH groups located at the periphery of the protein binding pocket, and exposed to solvent in solution, were found to participate in new protein−oligosaccharide hydrogen bonds in the gas phase. On the basis of the present results it is not possible to say whether the entire binding region underwent significant structural changes upon transfer to the gas phase or whether the changes were limited to the periphery. Further gas-phase studies of structurally related scFv−oligosaccharide complexes are needed to fully map the binding site in the gas phase.

The influence of charge on the dissociation pathways, kinetics, and energetics was also investigated. The $(scFv + \mathbf{2})^{n+}$ complex, where $n = 9-13$, served as a model system. Dissociation of

(36) Kitova, E. N.; Bundle, D. R.; Klassen, J. S. Unpublished results.

(37) Bundle, D. R. Recognition of carbohydrate antigens by antibody binding sites. In *Carbohydrates*; Hecht, S., Ed.; Oxford University Press Inc.: Oxford, 1998; pp 370−440.

the protonated complex, (scFv + **2** + *n*H)$^{n+}$, proceeded exclusively by the loss of neutral **2**. The stability (kinetic and energetic) of the complex decreased with increasing charge state (for $n = 10-13$). This result was attributed to conformational changes in the binding site, induced by electrostatic repulsion. Similar dissociation kinetics and energetics were measured for the +9 and +10 charge states, suggesting that the electrostatic effects may be negligible for $n \leq 10$. The attachment of one or more alkali metal ions to the complex resulted in a second, lower energy dissociation pathway involving the loss of **2**·M$^+$. The lower E_a was attributed to binding of the Na^+ ion directly to the oligosaccharide in the complex, resulting in a reduction of the number of stabilizing scFv−oligosaccharide interactions. Attachment of the Na^+ remote from the oligosaccharide resulted in the loss of neutral **2**, with Arrhenius parameters comparable to those measured for the protonated complex.

Finally, this work illustrates the potential of gas-phase dissociation studies, carried out under well-defined experimental conditions, in conjunction with a functional group replacement approach as an assay of intermolecular interactions in desolvated protein−ligand complexes. This approach can provide new and hitherto, unavailable insight into the nature and strength of protein−ligand interactions in the absence of solvent. Comparison of the binding interactions in solution and the gas phase will ultimately provide new insight into the role of solvent on binding and structure. The gas-phase data will also provide useful tests of, and aid in, the development of improved force fields suitable for gaseous biomolecules and biomolecular complexes.

Acknowledgment. We are grateful for financial support provided by the Natural Sciences and Engineering Research Council of Canada (NSERC) and Thermoquest through sponsorship of the American Society for Mass Spectrometry 2000 Research Award (J.S.K.). We thank M. Klobukowski for assistance with the computational studies.

Supporting Information Available: Cartesian coordinates for the HF/6-31G** optimized structures of histidine, imidazole, β-galactose, and the imidazole-β-galactose complex and their corresponding energies and vibrational frequencies (PDF). This material is available free of charge via the Internet at http://pubs.acs.org.

JA017213O